Astron. Astrophys. 173, 352–360 (1987)

ASTRONOMY AND ASTROPHYSICS

A multilevel study of ammonia in star-forming regions

I. Maser and thermal emission toward W51 IRS 2

R. Mauersberger*, C. Henkel, and T.L. Wilson

Max-Planck-Institut für Radioastronomie, Auf dem Hügel 69, D-5300 Bonn 1, Federal Republic of Germany

Received July 24, accepted September 18, 1986

Summary. Observations of $^{14}NH_3$ and $^{15}NH_3$ thermal transitions toward W51 IRS 2, which show various excitation conditions, are presented. In addition to the $(J,K) = (6,3)$ and $(9,6)$ transitions (Madden et al., 1986), the $(J,K) = (5,4)$, $(7,5)$, $(9,8)$ and $(10,8)$ transitions show spike-like emission features and are probably masering. If so, this is the first detection of para NH_3 masers in outer space. The gas traced out by highly excited transitions of NH_3 arises in a compact ($2.4\,10^{-2}$ pc), hot ($T_{kin} \sim 300$ K) and dense ($n(H_2)_{vir} = 10^{7.7}\,cm^{-3}$) region, which is probably optically thick in the IR range up to $\sim 200\,\mu m$ and is heated by IRS 2. The masers may arise near the compact H II region W51d. We report the first detection of the $(J,K) = (11,9)$ transition of NH_3, which is 1446 K above the ground state.

Key words: atomic and molecular processes – interstellar medium: molecules – interstellar medium: abundances – masers – radio lines molecular – W51 IRS 2

1. Introduction

Observations of the inversion transitions of ammonia at a wavelength of ~ 1.3 cm have provided estimates of both the kinetic temperature and the density of molecular clouds. From the intensity ratios of the transitions within each K-ladder, H_2 densities can be estimated (Mauersberger et al., 1985). From the intensity ratios of the (J,J) levels of different K-ladders, rotational temperatures, T_{rot}, can be obtained. At high densities, the values of T_{rot} are close to the kinetic temperatures, T_{kin}, (Walmsley and Ungerechts, 1983). Kinetic temperature estimates range from ~ 10 K in dark clouds (Myers and Benson, 1983) to more than 300 K in compact molecular sources associated with H II regions (Mauersberger et al., 1986a). In some high density molecular sources seen in emission it has been observed that T_{rot}, obtained from pairs of metastable lines, increases with energy above the ground state (Mauersberger et al., 1986a). This may be due to temperature gradients or several components, with different T_{kin}, within the cloud. Toward Orion-KL, 27 lines of $^{14}NH_3$ and 7 lines of $^{15}NH_3$ between 20 K and 1200 K above the ground state have been observed (Hermsen et al., 1985; Hermsen, 1985). However, the blending of at least three gas components with different radial velocities and physical properties make the interpretation of the data difficult. The source W51 IRS 2 resembles the Orion-KL object in many respects (see e.g. Genzel et al., 1982), but has only one velocity component relevant for the study of highly excited molecular gas. Since the molecular cloud core W51 NH_3-3, observed in the direction of W51 IRS 2, has the highest column density of NH_3 found in the survey of Mauersberger et al. (1986a), we have measured additional NH_3 lines toward W51 IRS 2 in order to investigate the excitation conditions within this molecular cloud in more detail.

2. Observations

The observations were carried out in spring and autumn 1985 and spring 1986 with the Effelsberg 100-m telescope equipped with a K-band maser receiver. We used a 1024 channel autocorrelator, with 2 bit sampling, operated as two 512 channel spectrometers. We simultaneously observed the (4,4) and (10,9), the (5,4) and (4,3), the (7,5) and (10,8), the (8,6) and (9,7) lines of $^{14}NH_3$, the (3,2) line of $^{14}NH_3$ and the (3,3) line of $^{15}NH_3$, the (2,1) line of $^{14}NH_3$ and the (4,4) line of $^{15}NH_3$, and the (1,1) and (2,2) transitions of $^{15}NH_3$. The total bandwidth was either 12.5 or 25 MHz, the velocity resolution 0.4 or 0.8 km s^{-1} (see Table 1). The line rest frequencies (Poynter and Kakar, 1975; Hermsen et al., 1985) cover the range between 18.9 and 24.2 GHz. In this range, the FWHP beamwidth is $\theta = 5 + 27\lambda$ where θ is in arcseconds and λ, the wavelength, is in cm. The main-beam brightness temperature scale was based on continuum measurements of NGC 7027 and W3(OH) for which flux densities of 5.9 and 3.2 Jy were assumed. At Effelsberg, in the K-band range, the main beam brightness temperature corresponding to 1 Jy per beam follows the relation $T_{MB}/Jy = 1.80 - 0.016\nu$, where T_{MB} is in K and ν is in GHz. We employed position switching with integration times of 5^m per on-source measurement. The reference position was at -5^m of R.A. relative to the source ($\alpha_{1950} = 19^h21^m22^s.2$, $\delta_{1950} = 14°25'17''$).

3. Data reduction and results

In addition to 2 metastable inversion transitions, we detected 16 non-metastable inversion lines of $^{14}NH_3$ (up to J = K + 3) and 4 lines of $^{15}NH_3$ toward W51 IRS 2. Among these is the first astronomical detection of the (11,9) line of ammonia. It is 1446 K above the ground state and is thus the ammonia line

Send offprint requests to: R. Mauersberger

* Present address: I.R.A.M., Av. Divina Pastora 7, Nucleo Central, E-18012 Granada, Spain

Table 1. Line parameters of $^{14}NH_3$ toward W51 IRS 2

(J,K)	Date	Velocity[d] resolution ($km\,s^{-1}$)	T_{MB} (K)	v_{LSR} ($km\,s^{-1}$)	$\Delta v_{1/2}$ ($km\,s^{-1}$)	τ_{tot}	$N(J,K)/T_{ex}$[e] ($10^{13}\,cm^{-2}/K$)
(1, 1)[a,c]	84/04/28	0.2	0.85(0.05)	51.2 (0.1)	6.8 (0.4)	<0.5	
			2.1 (0.1)	60.3 (0.1)	5.8 (0.1)	2.6(0.2)	21.0(2.0)
(2, 2)[a,c]	84/04/28	0.2	0.62(0.05)	52.3 (0.3)	8(1)	<0.8	
			2.0 (0.1)	60.4 (0.1)	4.8 (0.1)	2.8(0.2)	14.0(1.2)
(3, 3)[a]	85/09/29	0.4	1.3 (0.1)	58.9 (0.2)	8.7 (0.2)	3.6(0.5)	29(4)
			1.1 (0.2)	60.4 (0.2)	6(1)		
(4, 4)[a]	85/09/29	0.4	0.61(0.02)	60.2 (0.2)	5.2 (0.3)	10(2)	44(12)
(5, 5)[a,c]	83/02/21	0.8	0.60(0.02)	59.5 (0.2)	~5	20(2)	80(20)
(7, 7)[a,c]	84/08/27	0.8	0.31(0.01)	60.4 (0.1)	5.1 (0.1)	32(3)	119(12)
(2, 1)[a]	86/03/30	0.4	0.32(0.01)	60.5 (0.1)	5.7 (0.2)	10.1(0.7)	246(30)
(3, 2)[b]	85/09/29	0.4	0.48(0.03)	59.9 (0.2)	9.2 (0.5)	7.1(3.7)	80(30)
(4, 3)[a]	85/09/29	0.4	0.44(0.02)	59.9 (0.2)	4.7 (0.4)	37(7)	281(60)
(5, 4)[a]	85/09/29	0.4	0.34(0.02)	60.3 (0.3)	5.5 (0.3)	46(4)	346(60)
			0.70(0.06)	57.1 (0.1)	1.8 (0.3)		
(6, 5)[b]	85/09/27	0.8	0.30(0.02)	59.3 (0.3)	11(1)	23(12)	140(80)
(7, 6)[b]	85/09/27	0.8	0.25(0.02)	60.6 (0.4)	10.8 (1.0)	39(16)	220(90)
(8, 7)[b]	85/09/23	0.8	0.29(0.03)	60.9 (0.4)	8.8 (1.0	16(10)	85(50)
(9, 8)	85/09/29	0.4	0.20(0.03)	59.9 (0.5)	6.7 (1.1)		
			3.1 (0.3)	55.51(0.02)	0.38(0.04)		
	86/03/30	0.05	2.8 (0.1)	55.43(0.01)	0.44(0.02)		
(10, 9)	85/09/29	0.4	0.14(0.03)	59.7 (0.7)	6.6 (1.6)		
(4, 2)	85/11/01	0.4	0.22(0.2)	60.5 (0.6)	14.9 (1.5)		
(6, 4)	85/10/04	0.8	0.40(0.03)	60.0 (0.6)	11(1)		
(7, 5)	86/03/30	0.4	0.14(0.01)	60.8 (0.6)	12.1 (1.4)		
		0.1	0.14(0.05)	55.4 (0.1)	0.76(0.3)		
(8, 6)[a]	86/03/30	0.4	0.23(0.01)	62.0 (0.3)	5.7 (0.3)	100(30)	906(300)
(9, 7)	86/03/30	0.4	0.12(0.01)	61.4 (0.5)	11.8 (1.2)		
(10, 8)	85/10/04	0.8	0.18(0.03)	56(1)	11(2)		
	86/03/30	0.1	0.90(0.08)	55.43(0.02)	0.43(0.05)		
(11, 9)	85/09/20	0.8	0.13(0.3)	58(1)	8.3 (2.6)		
(13, 11)	85/10/25	0.4	<0.1				
(4, 1)	85/03/01	0.4	<0.15				
(5, 2)	85/10/25	0.4	0.16(0.02)	60.1 (0.4)	8.8 (1.0)		
(6, 2)	85/10/26	0.4	<0.15				

[a] The line parameters and the optical depths were obtained from a least-squares fit to the HF components
[b] The optical depth and column density was estimated by fixing the unsaturated linewidth of a single HF component
[c] Adopted from Mauersberger et al. (1986a)
[d] The autocorrelator was split into two receivers except for the (4, 1) line
[e] Averaged over the source

with the highest energy above the molecular ground state detected in interstellar space. So far, including previous observations (e.g. Mauersberger et al., 1985; Mauersberger et al., 1986a), in total 6 metastable and 19 non-metastable lines of $^{14}NH_3$ have been detected toward IRS 2. In Table 1, the line parameters are listed, the line profiles are shown in Fig. 1a. A least-squares fit to the HF components has been applied to those transitions of $^{14}NH_3$ which have a sufficient signal-to-noise ratio to show the hyperfine (HF) components. The relative intensities and separations were calculated using the formalism described by Mauersberger (1983) and the molecular constants supplied by Hougen (1972). They are, for some transitions tabulated in Hermsen (1985), e.g. for the (5, 4) line, the unsaturated intensity of a quadrupole HF satellite is predicted to be 1% that of the main line. So the presence of measurable HF satellites in the profiles of the highly excited transitions indicates very large optical depths. For the (8, 6) line, the unsaturated relative intensity of a single quadrupole satellite is 0.47% and the relative separations are ± 0.88 MHz ($12.7\,km\,s^{-1}$) and ± 0.68 MHz ($9.8\,km\,s^{-1}$). Hyperfine structure could be measured for the metastable transitions and in the (2, 1), (4, 3), (5, 4) and (8,6) lines. The profile of the (8, 6) line together with the fit to the HF satellites is shown in Fig. 1b. It might be thought that the velocity structure mimics HF structure. If so, this structure should be observed in other transitions, which is not the case. Since the (5, 4) line has at least two velocity components, the determination of the optical depth is difficult and should be regarded with some caution. The fit to the HF satellites was made after subtraction of a narrow spike-like feature

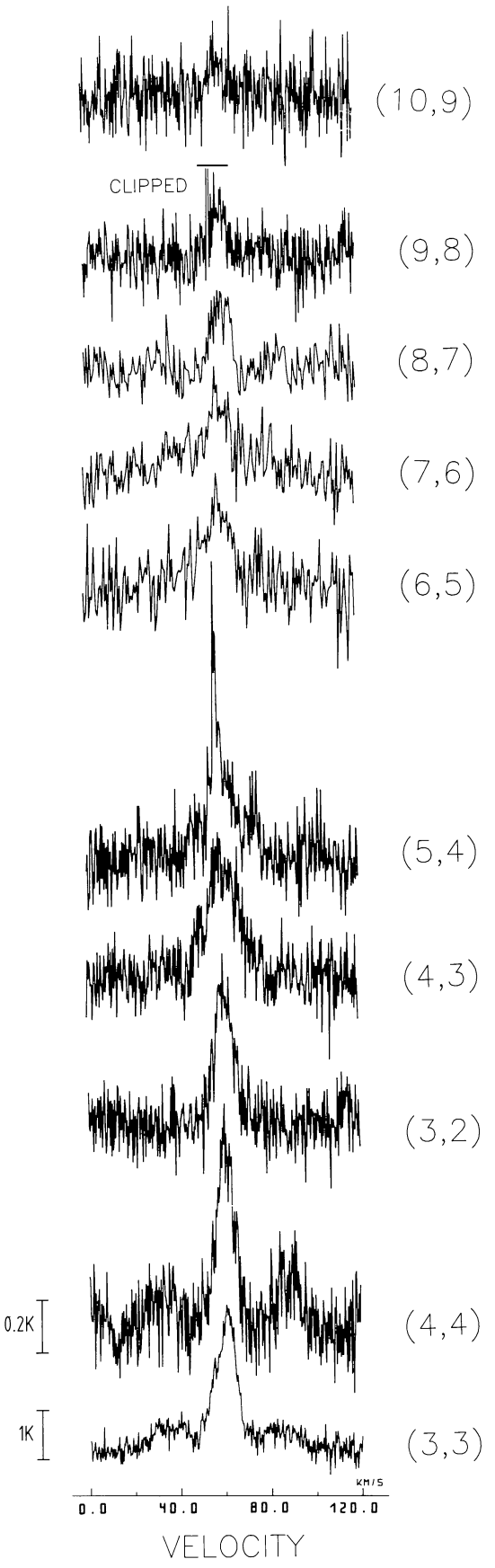

Fig. 1a. The $^{14}NH_3$ profiles toward W51 IRS 2. Some further $^{14}NH_3$ profiles can be found in Mauersberger et al. (1985, 1986a). In order to show the thermal component, we have clipped the maser peak in the profile of the (9, 8) line

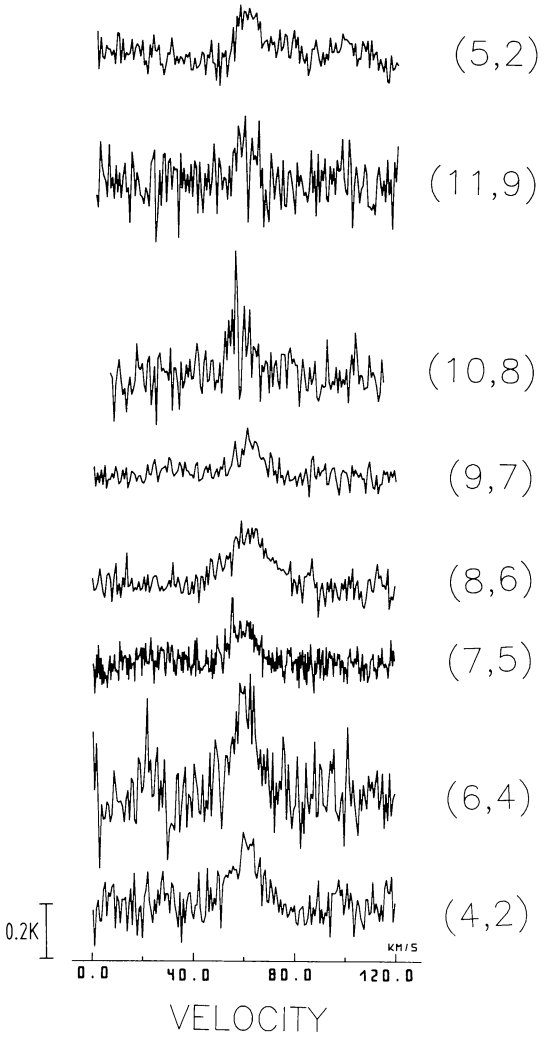

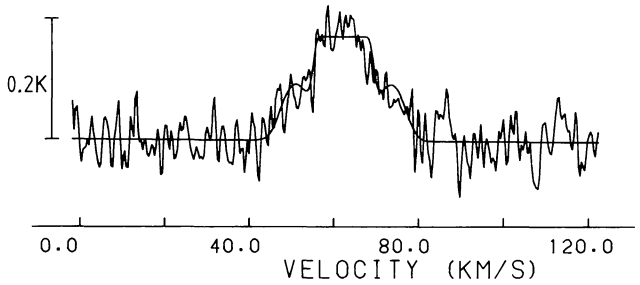

Fig. 1b. A least-squares fit (smooth line) to the HF components is superimposed on the profile of the (8,6) line. From the intensity ratios the optical depth is 100(±30)

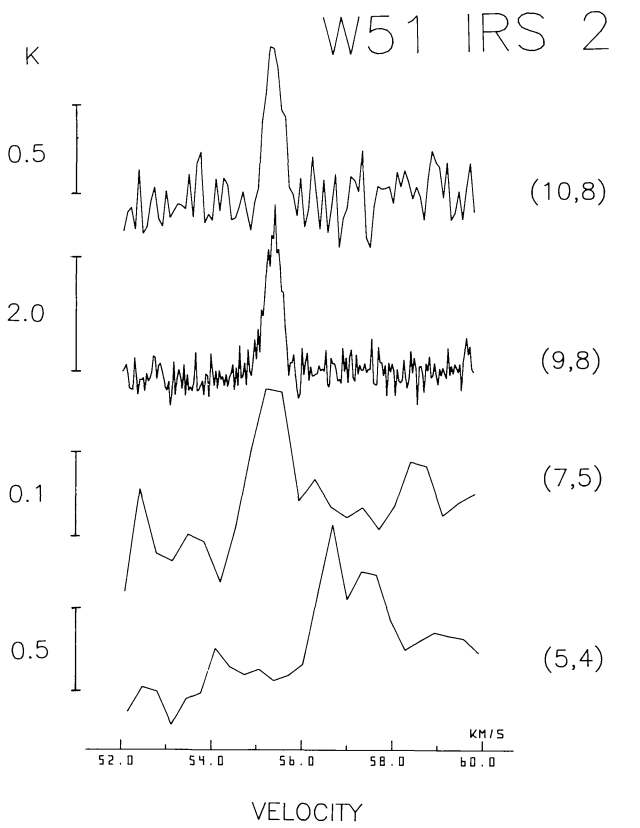

Fig. 1c. The (5,4), (7,5), (9,8) and (10,8) maser profiles. The velocity resolution is 0.32, 0.35, 0.039 and 0.088 km s^{-1} respectively

at 57.1 km s^{-1}. For these lines the value for $\Delta v_{1/2}$ is the unsaturated line width of a single HF component; we also give the total optical depth, i.e. the sum of all HF components. Since the (3,2) line has no quadrupole HF satellites, no optical depth could be determined from the HF satellite ratio. For this, and the (6,5), (7,6) and (8,7) transitions, we have fixed the unsaturated linewidth of a single HF component to the value of 5.1 km s^{-1}, given by Mauersberger et al. (1986a) for the (7,7) line, in order to set some limits to τ. We have applied a Gaussian fit to the remaining profiles. For these, $\Delta v_{1/2}$ is the apparent FWHP width of the lines. For some non-metastable lines, the HF satellites are so close to the main group of HF components that they are not resolved in the optically thick case. We have fit two Gaussians to the (9,8) and (7,5) transitions in order to take into account the narrow features observed on a broader emission profile. In the (9,8) transition, we made a 5-point cross raster with 20″ spacing centered on W51 IRS 2 in order to determine the size and location of the spike-like emission feature. These data are consistent with the assumption that the region of maser emission is smaller than 20″ and centered within 10″ on W51 IRS 2.

The total column density of the inversion levels (J,K) of ammonia is

$$N(J,K) = (1.65\,10^{14}/\nu)(J(J+1)/K^2)\Delta v_{1/2}\tau_{\rm tot}T_{\rm ex} \quad (1)$$

where N is in cm^{-2}, the inversion frequency ν is in GHz, the unsaturated line width $\Delta v_{1/2}$ is in km s^{-1}, and the excitation temperature $T_{\rm ex}$ is in K. Given $\Delta v_{1/2}$, $\tau_{\rm tot}$ and $T_{\rm ex}$, column densities can be determined. In Col. (8) of Table 1, we list the column densities of $^{14}NH_3$ averaged over the source divided by $T_{\rm ex}$ for those transitions for which we have an estimation of τ; in Col. (7) of Table 2 we give the column densities of the $^{15}NH_3$ transitions averaged over the beam, assuming that they are optically thin.

4. Discussion

4.1. Nomenclature and morphology of the region containing W51 IRS 2

We take a distance of 7.8 kpc for W51 IRS 2 (Georgelin and Georgelin, 1976); at this distance, 1″ is 3.8 10^{-2} pc (1.2 10^{17} cm). W51 consists of several discrete sources embedded in a continuum background. At 6 cm, the two most intense components are

Table 2. Line parameters of $^{15}NH_3$ toward W51 IRS 2

(J,K)	Date	Velocity resolution[a] (km s^{-1})	$T_{\rm MB}$[b] (mK)	$v_{\rm LSR}$ (km s^{-1})	$\Delta v_{1/2}$ (km s^{-1})	N[c] (10^{13} cm^{-2})
(1,1)	85/09/20	0.8	85(20)	59.3(0.4)	3.8(0.9)	0.47(0.15)
(2,2)	85/09/29		110(10)	61.5(0.4)	6.9(0.9)	0.82(0.15)
(3,3)	85/09/28 85/09/29	0.4	170(10)	58.7(0.3)	9.3(0.9)	1.52(0.23)
(4,4)	86/03/30	0.4	50(10)	60.8(0.6)	5.7(1.3)	0.24(0.10)
(6,6)	86/07/15	0.4	<80			<0.3
(7,7)	85/09/11	0.4	<100			<0.8

[a] Except for the (7,7) line, the autocorrelator was split into two channels
[b] From Gaussian fits to the lines
[c] Averaged over the beam

G49.5–0.4 and G49.5–0.3. These are called W51A. Maps by Martin (1972) resolved it into eight discrete compact sources, designed as W51 a–h. Toward the strongest of these sources (W51e and W51d), Wynn-Williams et al. (1974) detected the near IR emission sources W51 IRS 1 (near W51e) and W51 IRS 2 (near W51d). W51e is 45″ SE of W51d. 20″ east of W51e, Scott (1978) found two ultracompact radio sources (diameter ~2″) separated by 8″, which he called W51e$_1$ and W51e$_2$. Near (but not coincident with) W51e$_1$, W51e$_2$ and W51d, Ho et al. (1983) found, from VLA observations, hot compact ammonia emission. These clumps are named NH_3-1 (near W51e$_1$), NH_3-2 (near W51e$_2$) and NH_3-3 (near W51d). The labels were, however, exchanged for W51e$_1$ and W51e$_2$ in their 1.3 cm continuum map. From a map of the $(J,K) = (5,5)$ emission of NH_3 (293 K above the ground state), Mauersberger et al. (1986a) confirmed that the hot NH_3 is located toward W51e$_1$/e$_2$ and W51d (IRS 2) but not toward W51e (IRS 1). In the infrared, IRS 2 shows two peaks named IRS 2-West and IRS 2-East (Genzel et al., 1982). The position of IRS 2-West is coincident with the compact H II region W51d. The peaks of the 8 μm and 20 μm continuum at IRS 2-East coincide within the error limits with the position of the hot ammonia source NH_3-3 and the dominant center of the H_2O maser emission W51-North (Schneps et al., 1981). There is only a small, if any, overlap between the NH_3 and the compact H II region W51d (see Fig. 3b. in Ho et al. (1983)). The hot NH_3 emission has a radial velocity of 60 km s^{-1} (this paper). SiO and HCO^+ emission are peaked at 61 km s^{-1} with an FWHP line-width of 7–10 km s^{-1} (Downes et al., 1982). From observations of E-type methanol, Menten et al. (1986) find a v_{LSR} of 60 km s^{-1} and $T_{kin} = 60$ K. The H 109α radial velocity toward W51d is 56.4 km s^{-1} (Wilson et al., 1979).

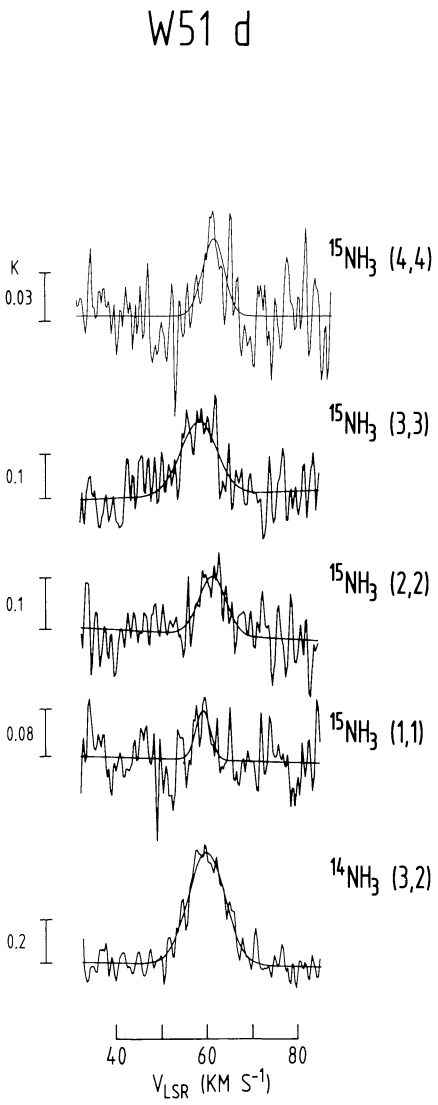

Fig. 2. The $^{15}NH_3$ profiles toward W51 IRS 2

4.2. *Kinetic temperature and column density*

The discussion of the temperature and size of the molecular gas toward W51 IRS 2 in Mauersberger et al. (1986a) was based on few lines. Our multilevel observations put their results on a firmer basis. Using the $^{14}NH_3$ transitions for which we obtained an estimate for τ and, hence, the column densities, we have made a Boltzmann plot, i.e. plotted $\log_{10}[(N/f\,T_{ex}/(g_{op}(2J+1))]$ versus the energy above ground (Fig. 3a). g_{op} is 2 for K = 3, 6, ..., otherwise g_{op} is 1; $f = T_{MB}/T_{ex}$ in the optically thick case is the beam filling factor. If all transitions have the same T_{ex}, the slope of a fit is $-0.434/T_{rot}$, where T_{rot} is the rotational temperature (see e.g. Walmsley and Ungerechts 1983). From a Boltzmann fit to those transitions for which we have an estimation of N, we obtain a common value for T_{rot} of 310(±40) K. An exception is the (8, 6) line, 833 K above ground. This line has, from the HF components, an optical depth of 100(±30), the largest value found for an interstellar ammonia inversion line and much larger than the value of ~20, which would be expected from the fit in Fig. 3a if the (8, 6) line were in LTE. The extremely large optical depth obtained for the (8, 6) line may result from subthermal (i.e. $T_{ex} \ll T_{kin}$) excitation in some parts of the cloud: since $T_{ex}\,\tau \propto N$, this results in an enhanced optical depth. The non-metastable levels are significantly populated, so that T_{ex} and T_{rot} should, in most cases, be close to the gas kinetic temperature T_{kin}. The value obtained for T_{rot} is an average over the hot ammonia source. The rotational temperature derived from the (1, 1) and (2, 2) lines is 60 K. Thus, there may be temperature and density gradients within our beam. The detection of ammonia line emission from levels more than 1000 K above the ground levels confirms that the temperatures must be very large toward IRS 2. From the Boltzmann fit, the total column density of $^{14}NH_3$ toward W51 IRS 2 (i.e. ortho and para ammonia), assuming an LTE population of metastable and non-metastable levels, with $T_{rot} = 310(\pm 40)$ K, is 6.8(±0.6) 10^{16} cm^{-2} T_{ex}.

4.3. *Size and gas density of the emission line region*

Mapping of the (1, 1), (2, 2) and (3, 3) lines of ammonia shows spatially extended emission toward W51 (Matsakis et al., 1980, Hermsen, unpublished). A map in the (5, 5) line shows that the hotter molecular gas is not resolved by the 40″ Effelsberg beam and is located toward W51e$_1$/e$_2$ and W51 IRS 2 (Mauersberger et al., 1986a). From the HF ratios, the lower lying metastable ammonia lines are moderately optically thick. We conclude that they sample a cooler, less dense component filling a larger volume than the gas observed in the transitions requiring higher excitation. H_2 densities larger than 10^5 cm^{-3} or far IR fields are necessary to populate the non-metastable levels of ammonia.

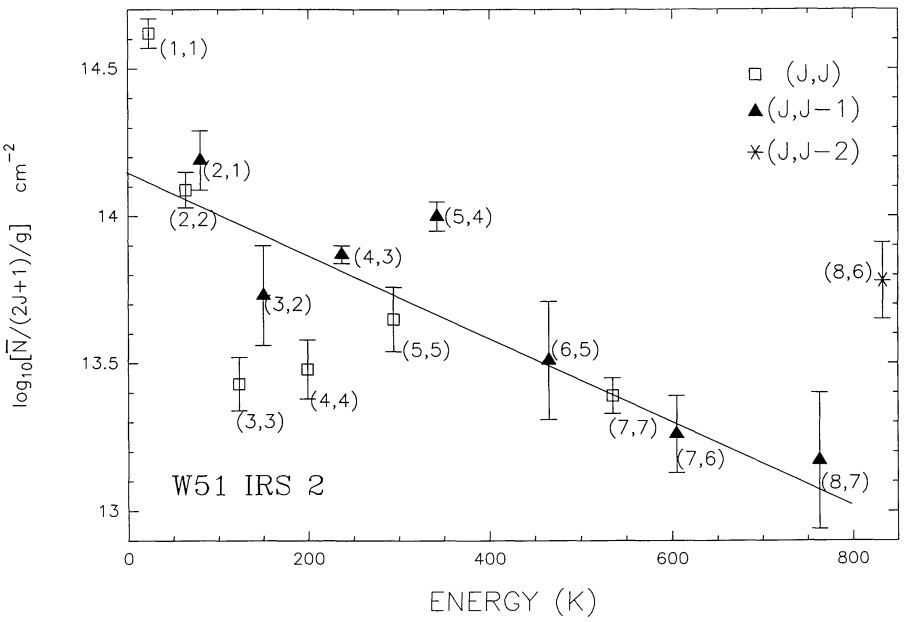

Fig. 3a. A Boltzmann plot for those $^{14}NH_3$ transitions for which we have an estimate of the optical depth. We have plotted $\log_{10}[NT_{MB}/T_{ex}/(2J+1)/g_{op}]$ versus the excitation energy. Since, in the optically thick case, T_{MB}/T_{ex} is the beam filling factor, $\bar{N} = NT_{MB}/T_{ex}$ is the beam averaged column density. The optical depth was estimated either from the ratio of the HF satellites or, in the case of the (3, 2), (6, 5), (7, 6) and (8, 7) lines from the line shape assuming an intrinsic FWHP line width of 5.1 km s^{-1}. From the slope of the correlation, T_{rot} is 310(±40) K. The metastable levels are indicated by open squares, the non-metastable ones with $(J - K) = 1$ by filled triangles and the (8, 6) level by an asterisk

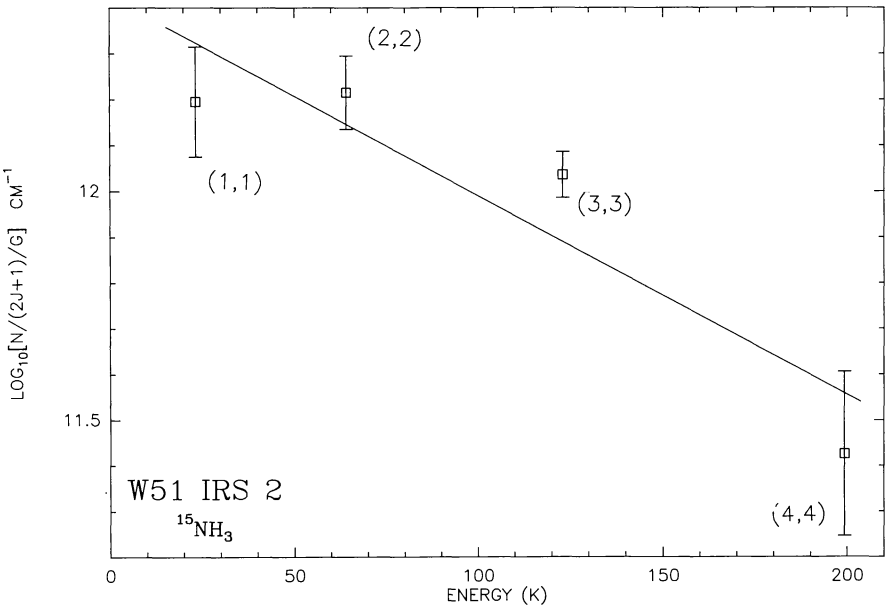

Fig. 3b. A Boltzmann plot for the $^{15}NH_3$ transitions. From the least-squares fit to the data, indicated by a line, $T_{rot} = 95(\pm 10)$. T_{rot} may increase for higher levels, but from the non-detection of the (6, 6) line, $T_{rot} \leq 150$ K

Thus, there must be one or more hot and dense ammonia clumps immersed in a more extended, cooler molecular gas. We believe that this hot and dense molecular gas is identical with the compact ammonia source NH_3-3 seen by Ho et al. (1983). Note, however, that their brightness temperature scale has to be revised (Mauersberger et al., 1986a). Mauersberger et al. (1985, 1986a) have found large optical depths in the (5, 5), (7, 7) and (2, 1) transitions. Large optical depths are also found in the (4, 4), (4, 3), (5, 4) and (8, 6) transitions, from fits to the HF components.

For a homogeneous slab, the main beam brightness temperature is

$$T_{MB} = f(T_{ex} - T_{BG})(1 - \exp(-\tau_{mg}) \quad (2)$$

where f is the beam filling factor, T_{ex} and T_{BG} are the excitation temperature respectively the background temperature and τ_{mg} is the optical depth of the main group of HF components. From the VLA map (Ho et al., 1983), the compact molecular cloud does not overlap with the compact H II region, so T_{BG} may be neglected. In the optically thick case, $T_{MB} \sim f T_{ex}$, i.e. a source size can be given from the knowledge of T_{ex}. If the non-metastable levels of ammonia are populated, $T_{ex} \sim T_{kin} \sim T_{rot}$ for metastable transitions. (see e.g. Mauersberger et al., 1985).

If one assumes that the lines are optically thick and $T_{ex} \sim T_{kin}$, different beam filling factors are responsible for the observed variations of T_{MB}. The size of the region of hot gas can be calculated from the beam filling factor in Eq. (2). With $T_{ex} =$ 310 K, for the (7, 7) line emitting region, we find from Eq. (2) a radius of 0.″63 or $2.4\,10^{-2}$ pc ($7.4\,10^{16}$ cm at a distance of 7800 pc) and $N(NH_3) = 2.1(\pm 0.5)\,10^{19}$ cm^{-2}, averaged over the source. We will use these values for r, the radius, and T_{kin} in the con-

text, although there may be an inhomogeneous temperature and density distribution within the source. The (4, 4) and (5, 5) lines are probably, like the (1, 1), (2, 2) and (3, 3) emission blended with a more extended cooler component. From the column density and an assumed spherical symmetry, the ammonia space density $n(NH_3) = 380\,cm^{-3}$. Using the solar H/N abundance ratio of 8500 (Allen, 1973) as a lower limit for $[H/NH_3]$, the density of molecular hydrogen, $n(H_2) \geq 10^{6.2}\,cm^{-3}$ (i.e. $N(H_2) \geq 10^{23}\,cm^{-2}$). The total molecular gas mass would then be $\geq 5\,M_\odot$. If the virial theorem can be applied, i.e. if the gravitational forces are balanced by the kinetic motions, the virial mass is $160\,M_\odot$ and the virial density is $10^{7.7}\,cm^{-3}$ (i.e. $N_{vir}(H_2) = 3\,10^{24}\,cm^{-2}$). With this H_2 density, the NH_3/H_2 abundance is $\sim 10^{-5.2}$. The NH_3/H_2 abundance in dark clouds is 10^{-7} (Ungerechts et al., 1980). The enhanced ammonia abundance could be explained by evaporation of ammonia from grains above 80 K (Sweitzer, 1978). If the A_V/E_{B-V} relation (Bohlin et al., 1978) obtained for the interstellar gas with $A_V < 2^m$ can be extrapolated to the high density cloud cores, the column density of H_2 obtained from the virial theorem corresponds to a visual extinction $A_V \sim 3000^m$. This large visual extinction implies that the cloud is optically thick for $\lambda < 200\,\mu m$. Harvey et al. (1986) estimated the optical depth at $100\,\mu m$ toward IRS 2 to be ~ 0.4. But this estimate is an average over their 25″ beam. From the source size and T_{kin}, we obtain a clump luminosity of $L = 5(\pm 2)\,10^6\,L_\odot$ using the Stefan-Boltzmann relation. This is close to the bolometric luminosity of $3\text{–}4\,10^6\,L_\odot$ estimated by Thronson and Harper (1979) and Erickson and Tokunaga (1980) for IRS 2. This leads to the conclusion that the heating source of the hot NH_3 is very close, possibly inside the hot molecular gas clump. The observed IR flux arises in a larger volume than the hot NH_3. Since the gas seen in the lower transitions of NH_3 is farther away from the heating source, its temperature is only ~ 60 K, i.e. near the dust color temperature of ~ 50 K (Harvey et al., 1986). This dust heats the extended warm gas seen in the lower lying NH_3 transitions.

4.4. The $^{14}NH_3/^{15}NH_3$ abundance ratio

We have also detected emission from the (1, 1), (2, 2), (3, 3) and (4, 4) lines of $^{15}NH_3$ and obtained a limit for the (7, 7) line. We assume that the $^{15}NH_3$ lines are optically thin, since their T_{MB} are substantially smaller than the corresponding T_{MB} of the main isotope. In this case, beam averaged column densities can be given, since $f T_{ex} \tau \sim T_{MB}$. We have made a Boltzmann plot (Fig. 3b), using the column density calculated this way. From the data, $T_{rot} \sim 95(\pm 10\,K)$. From the non-detection of the (6, 6) line of $^{15}NH_3$, $T_{rot} < 150$ K. This value is substantially lower than the estimates for T_{kin} from the main isotope. Since the non-metastable levels of $^{15}NH_3$ are perhaps not populated because of the low optical depth of this isotope, depopulation of the metastable levels via the nonmetastable states may make T_{rot} smaller than T_{kin} (see e.g. Walmsley and Ungerechts, 1983). From the model calculations of Mauersberger et al. (1986b), for hot (~ 200 K) and optically thin NH_3, $T_{rot} \sim 1/2 T_{kin}$ if $n(H_2) \leq 10^8\,cm^{-3}$. This is compatible with the virial density estimated above. The cooler gas may contribute significantly to the observed line intensities of $^{15}NH_3$. The determination of the total column density of $^{15}NH_3$ and, hence, the $^{14}NH_3/^{15}NH_3$ abundance also depends critically on the population of the non-metastable ammonia levels. This requires information about the H_2 density and the IR continuum radiation since either can excite NH_3 to non-metastable states. If we *assume* a common rotational temperature of 95 K for all metastable levels of $^{15}NH_3$ and if the non-metastable levels are not populated, the beam averaged column density of $^{15}NH_3$ is $\sim 3.5(\pm 0.9)\,10^{13}\,cm^{-3}$. If the metastable and $(J+1, J)$ levels are populated, which for $^{15}NH_3$ is the case for $n(H_2) > 10^8\,cm^{-2}$ (without excitation by FIR continuum) Mauersberger et al., 1986b) the beam averaged column density is $5.8(\pm 1.5)\,10^{13}\,cm^{-12}$. Using the column density and source size of the $^{14}NH_3$ emission estimated above, the corresponding $^{14}NH_3/^{15}NH_3$ abundance ratios are $660(\pm 300)$ if only the metastable $^{15}NH_3$ levels are populated and $400(\pm 200)$ if also the first non-metastable levels have to be taken into account. For $T_{rot} = 150$ K, we obtain similar results. These isotope ratios are within the range of 200 to 1000 determined by Güsten and Ungerechts (1985), Hermsen et al. (1985) and Mauersberger et al. (1986b). The width of the (3, 3) line of $^{15}NH_3$ is larger than that of the other $^{15}NH_3$ lines toward W51d and also larger than the unsaturated line width of the $^{14}NH_3$ lines. This may be caused by anomalous excitation in the line wings.

4.5. The ammonia maser emission toward W51 IRS 2

Model calculations (Walmsley and Ungerechts, 1983) predict that the (3, 3) line of ortho ammonia should be masering for a range of cloud parameters. Masering in the (3, 3) transition has been found toward W33 (Wilson et al., 1982) and DR21 (Guilloteau et al., 1983). Mauersberger et al. (1986b) detected the first $^{15}NH_3$ maser in outer space toward the compact H II region NGC 7538 IRS 1. The pump mechanism for a (3, 3) maser seems to be explained if the parity selection rules from the theoretically computed collisional cross sections by Green (1982) hold. No convincing explanation has been found for the (9, 6) and (6, 3) masers reported toward W51 by Madden et al. (1986). Another para-ammonia maser in the (6, 5) line has been reported toward W3(OH) (Mauersberger et al., 1986c). Our profiles show spike-like emission in the (5, 4), (7, 5), (9, 8) and (10, 8) transitions (Fig. 1c), which are not seen in any of the other quasi thermally excited lines toward W51 IRS 2. These features must be produced by a non-LTE process, probably a maser, since (1) the thermal linewidth of these spikes are smaller than $0.9\,km\,s^{-1}$, the thermal linewidth of 300 K ammonia and (2) no comparable features are found in other transitions. Between September 1985 and March 1986, the T_{MB} of the (9,8) maser remained constant. If the (9, 8) line covers and amplifies the continuum of W51d, for which Ho et al. (1983) derived a total flux density of 2.8 Jy at 1.3 cm, its optical depth is -0.7. A possible pump mechanism for non-metastable NH_3 masers is the transfer of the population from the lower (J, K) inversion level to the upper $(J+1, K)$ inversion level (Fig. 4) by an IR field or an accidentally overlapping FIR line. In the Appendix, we derive as a condition for masering that $T_{rot} > 2T_{ex}$. We have found evidence that the (8, 6) line is subthermally excited (see Sect. 4.2) while Madden et al. (1986) observed strong maser emission in the (9, 6) line at 51.0, 54.2, 58.4, 61.0 and $62.0\,km\,s^{-1}$. This fact may give support to the above simple model. We observe, however, spike-like (presumably maser) emission in two adjacent inversion transitions of a K-ladder, namely the (9, 8) and (10, 8) lines, which is unexpected from our model if both lines arise in the same volume as suggested by the velocities and linewidths. This indicates that the maser scheme is more complicated: perhaps vibrationally excited levels of ammonia have to be taken into account in order to explain the maser mechanism. The (7,5), (9,8) and (10,8) maser lines have the same

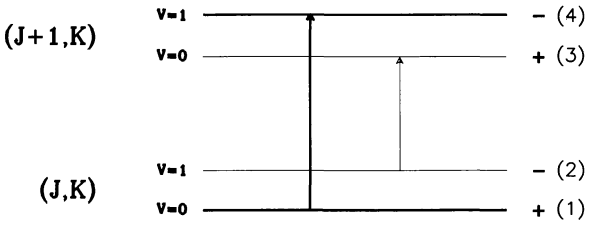

Fig. 4. A schematic diagram of the (J,K) and $(J+1,K)$ levels of NH_3. Dipole transitions involve a parity change. Pumping via the accidental overlap with a line from another molecule or an intense IR continuum together with photon trapping can transfer population of level 1 to level 4 and invert the $(J+1,K)$ inversion levels

radial velocity and line width (55.4 and 0.4 km s^{-1}) and, hence, probably arise in the same region while the (5,4) line is at 57.1 km s^{-1}. The radial velocities of the masers are close to that of the H109α emission at 56.4 km s^{-1} of W51d (Wilson et al., 1979). No absorption at the radial velocities of these masers has been observed in any of the ammonia inversion lines. So, the column density of the masering NH_3 gas located in front of the H II region must be small. If the masers are near W51d, the IR field by the H II region may play a significant role in the maser pump scheme. Whether a non-metastable inversion line is actually masering may depend critically on the cloud parameters (i.e. $n(H_2)$, $n(NH_3)$, T_{kin}, IR-field).

5. Conclusions

The main points presented in this paper are:

(1) The ammonia seen in highly excited transitions toward W51 IRS 2 arises in a compact ($r = 2.4\,10^{-2}$ pc), hot ($T_{kin} = 310\ (\pm 40)$ K and dense ($n_{vir}(H_2) = 10^{7.7}$ cm^{-3}) region with an enhanced NH_3/H_2 abundance ($10^{-5.2}$).

(2) This clump is optically thick in the IR range up to 200 μm and is heated by IRS 2.

(3) We have detected maser emission in the (5,4), (7,5), (9,8) and (10,8) transitions. These are the first para ammonia masers detected in outer space. The emission may arise in front of or near W51d.

(4) The proposed pump mechanism transfers the population of the lower (J,K) inversion level to the upper $(J+1,K)$ level. This may be due to accidently overlapping infrared lines or an intense FIR field together with photon trapping. An alternative mechanism involves the vibrationally excited states of ammonia.

(5) We have first detected the (11,9) line of NH_3 in interstellar space. With 1446 K above the ground state, this is the inversion transition with the highest excitation energy known in the interstellar medium.

6. Appendix: The inversion of the (J,K) levels

In a simple 2-level model, we deduce a condition for masering of the (J,K) inversion level of ammonia. The maser pump process may be closely connected to the population of the rotationally excited levels within a K-ladder. These excited states decay rapidly. The A-coefficient for spontaneous decay from a (9,8) to the corresponding (8,8) level is 0.19 s^{-1}. In order to account for infrared photon trapping, an effective A-coefficient must be defined. If β is the escape probability of a line photon, the rate coefficient for self absorption in the line is $A(1-\beta)$, where A is the Einstein coefficient for spontaneous emission. This value must be subtracted from A to get the effective A: $A_{eff} = \beta A$. For simple geometries, β may be evaluated. For a homogeneous slab, $\beta = (1-\exp(-3\tau))/3\tau$ and for a spherical cloud, $\beta = (1-\exp(-\tau)/\tau$ (Scoville and Solomon, 1974; Goldreich and Kwan, 1974), i.e. in the optically thick case, $\beta \sim 1/3\tau$ or $\beta \sim 1/\tau$. τ_{IR} is the optical depth of the IR rotational transition. It can be estimated that $\tau_{IR} \sim 100\tau_{inv}$, where τ_{inv} is the optical depth of the inversion transition. With an expected value for $\tau_{inv}(8,8)$ of at least ~20, τ_{rot} becomes >2000. A critical density for the population of the non-metastable levels can be estimated from $n_{crit}(H_2) = A_{eff}/\langle\sigma v\rangle$, where $\langle\sigma v\rangle$ is the rare constant for collisional deexcitation linking the two transitions where trapping occurs. Billing et al. (1985) do not provide collision rates for levels as high as the (8,8) line but only for transitions with $K \leq 3$. These are $\sim 5\,10^{-11}$ cm^3 s^{-1} for the deexcitation of a $(J+1,J)$ level to a (J,J) level. If we assume the same value also for the deexcitation of the corresponding (9,8) rotational transitions, we obtain, with $\tau_{rot} = 2000$, a critical density for the population of the (9,8) inversion doublets of $10^{6.3}$ cm^{-3}. The lower (J,K) level of NH_3 is linked with the upper $(J+1,K)$ level and the upper (J,K) level with the lower $(J+1,K)$ level via photon trapping (see Fig. 4). If the rotational temperature exceeds the excitation temperature of the (J,K) levels, the $(J+1,K)$ levels can be inverted. This behaviour has been found in the model by calculations by Walmsley and Ungerechts (1983) for the (2,1) transitions. The maser pump can be an IR field or accidently overlapping line radiation in the IR. We denote the populations of the lower and upper (J,J) levels with N_1 respectively N_2 and the lower and upper $(J+1,J)$ levels with N_3 respectively N_4 (Fig. 4). Then, the excitation temperatures between the inversion levels and the rotational temperatures between the rotational levels are defined by

$$N_4/N_3 = \exp(-\Delta E_{inv}/T_{ex}(J+1,J)) \quad \text{(A1a)}$$

$$N_2/N_1 = \exp(-\Delta E_{inv}/T_{ex}(J,J)) \quad \text{(A1b)}$$

$$N_3/N_2 = ((2J+3)/(2J+1))\exp(-\Delta E_{32}/T_{rot}) \quad \text{(A1c)}$$

$$N_4/N_1 = ((2J+3)/(2J+1))\exp((-\Delta E_{32} + 2\Delta E_{inv})/T_{rot}) \quad \text{(A1d)}$$

where ΔE_{inv} is the energy difference between two inversion states (~1.1 K) and ΔE_{32} is the energy difference between the rotational states. The Eqs. (A1) lead to

$$1/T_{ex}(J+1,J) = 2/T_{rot} - 1/T_{ex}(J,J) \quad \text{(A2)}$$

This implies that $T_{ex}(J+1,J)$ becomes negative if $T_{rot} > 2T_{ex}(J,J)$, if there is a single T_{rot} for the two sets of levels.

References

Allen, C.W.: 1973, Astrophysical Quantities, The Athlone Press, London

Billing, G.D., Poulsen, L.L., Diercksen, G.H.F.: 1985, *J. Chem. Phys.* **98**, 397

Bohlin, R.C., Savage, B.D., Drake, J.F.: 1978, *Astrophys. J.* **224**, 132

Downes, D., Genzel, R., Hjalmarson, Å., Nyman, L.Å., Rönnäng, B.: 1982, *Astrophys. J. Letters* **252**, L29

Erickson, E.F., Tokunaga, A.T.: 1980, *Astrophys. J.* **238**, 596

Genzel, R., Becklin, E.E., Wynn-Williams, C.G., Moran, J.M., Reid, M.J., Jaffe, D.T., Downes, D.: 1982, *Astrophys. J.* **255**, 527

Georgelin, Y.M., Georgelin, Y.P.: 1976, *Astron. Astrophys.* **49**, 57
Goldreich, P., Kwan, J.: 1974, *Astrophys. J.* **189**, 44
Guilloteau, S., Wilson, T.L., Martin, R.N., Batrla, W., Pauls, T.A.: 1983, *Astron. Astrophys.* **124**, 322
Güsten, R., Ungerechts, H.: 1985, *Astron. Astrophys.* **145**, 241
Harvey, P.M., Joy, M., Lester, D.F., Wilking, B.A.: 1986, *Astrophys. J.* **300**, 737
Hermsen, W.: 1985, Ph.D. Thesis, Bonn University
Hermsen, W., Wilson, T.L., Walmsley, C.M., Batrla, W.: 1985, *Astron. Astrophys.* **146**, 134
Ho, P.T.P., Genzel, R., Das, A.: 1983, *Astrophys. J.* **266**, 596
Hougen, J.T.: 1972, *J. Chem. Phys.* **57**, 4207
Madden, S.C., Irvine, W.M., Matthews, H.E., Brown, R.D., Godfrey, P.D.: 1986, *Astrophys. J.* **300**, L79
Martin, A.H.M.: 1972, *Monthly Notices Roy. Astron. Soc.* **157**, 31
Matsakis, D.N., Bologna, J.M., Schwartz, P.R., Cheung, A.C., Townes, C.H.: 1980, *Astrophys. J.* **241**, 655
Mauersberger, R.: 1983, Diploma Thesis, Bonn University (unpublished)
Mauersberger, R., Henkel, C., Wilson, T.L., Walmsley, C.M.: 1986a, *Astron. Astrophys.* **162**, 199
Mauersberger, R., Walmsley, C.M., Wilson, T.L., Henkel, C.: 1986c, *Mitt. Astron. Ges.* **65**, 190
Mauersberger, R., Wilson, T.L., Walmsley, C.M., Batrla, W., Walmsley, C.M., Henkel, C.: 1985, *Astron. Astrophys.* **146**, 168
Mauersberger, R., Wilson, T.L., Henkel, C.: 1986b, *Astron. Astrophys.* **160**, L13
Menten, K.M., Walmsley, C.M., Henkel, C., Wilson, T.L.: 1986, *Astron. Astrophys.* **157**, 318
Myers, P.C., Benson, P.J.: 1983, *Astrophys. J.* **266**, 309
Poynter, R.L., Kakar, R.K.: 1975, *Astrophys. J. Suppl.* **29**, 87
Schneps, M.H., Lane, A.P., Downes, D., Moran, J.M., Genzel, R., Reid, M.J.: 1981, *Astrophys. J.* **249**, 124
Scott, P.F.: 1978, *Monthly Notices Roy. Astron. Soc.* **183**, 435
Sweitzer, J.S.: 1978, *Astrophys. J.* **225**, 116
Thronson, H.A., Harper, D.A.: 1979, *Astrophys. J.* **230**, 133
Walmsley, C.M., Ungerechts, H.: 1983, *Astron. Astrophys.* **122**, 10
Wilson, T.L., Batrla, W., Pauls, T.A.: 1982, *Astron. Astrophys.* **110**, L20
Wilson, T.L., Bieging, J., Wilson, W.E.: 1979, *Astron. Astrophys.* **71**, 205
Wilson, T.L., Mauersberger, R., Walmsley, C.M., Batrla, W.: 1983, *Astron. Astrophys.* **127**, L19
Wynn-Williams, C.G., Becklin, E.E., Neugebauer, G.: 1974, *Astrophys. J.* **187**, 473